Ambient temperature performance of cementitious matrices for fire-safe NSM FRP strengthening of concrete structures

AMBIENT TEMPERATURE PERFORMANCE OF CEMENTITIOUS MATRICES FOR FIRE-SAFE NSM FRP STRENGTHENING OF CONCRETE STRUCTURES

Iolanda Del Prete[1], Antonio Bilotta[1], Luke Bisby[2], Emidio Nigro[1]

Department of Structures for Engineering and Architecture, University of Naples Federico II,
via Claudio 21 80125 Naples, ITALY
BRE Centre for Fire Safety Engineering, School of Engineering, University of Edinburgh
The King's Buildings, Edinburgh, EH93JL, Scotland, UK

ABSTRACT

The near surface mounted (NSM) fiber reinforced polymer (FRP) strengthening technique is a demonstrated, attractive and efficient alternative to externally bonded reinforcement (EBR) strengthening systems. NSM strengthening can be used to enhance the stiffness and the strength of deficient reinforced concrete members, with high utilisation of the FRP's mechanical properties (at ambient temperature) when epoxy is used as bonding agent. However, owing to epoxy adhesives' sensitivity to elevated temperature exposure, recent research has focused on the use of cementitious adhesives, which are less sensitive to elevated temperature, in NSM FRP applications. This paper presents results from 22 bond pull-out tests at ambient temperature on concrete prisms with an embedded carbon FRP bar NSM strengthening system. Different bonding agents (i.e. epoxy resin or cementitious grout), positions of the bar in the groove (i.e. in the centre or at the top of the groove), bar surface treatments (smooth and ribbed) and bond length (300 and 400 mm) are investigated.

KEYWORDS: NSM, FRP, cementitious adhesives, epoxy adhesives, bond tests, strengthening

1 INTRODUCTION

Near surface mounted (NSM) fibre-reinforced polymer (FRP) is a strengthening technique consisting of an FRP bar/rod/strip, which is bonded within a groove cut into the concrete cover of a reinforced concrete member, and bonded in place by filling the groove with a suitable bonding agent. The NSM strengthening technique is recognized as promising method for increasing flexural strength of reinforced concrete (RC) members, more convenient than using externally bonded FRP reinforcement (EBR) in some cases. NSM FRP strengthening has the advantages that is does not require any concrete surface preparation, except for cutting grooves in the concrete cover, which can be easily done in one step using suitable hand tools (such as a 'tuckpointing' grinder as known in North America). The choice of high-viscosity bonding agents, such as thixotropic resins, may be helpful during the groove's filling stage, but also more fluid products, such as cementitious pastes and crack-injection products, can also be used to grout the FRP strengthening material in place.

Despite of researchers are finding improvement for EBR systems (e.g. hybrid fiber reinforced polymer systems or hardwire steel-fiber sheets, [1],[2],[3]), on the other hand, several researchers have recognized the fact that NSM FRP strengthening systems present many potential advantages when compared to EBR systems [4],[5]. El Hacha & Rizkalla, 2004 [6] noted that the larger bonding surface of certain NSM products (strips in particular) gives superior anchorage capacities, providing higher resistance against peeling-off, and enabling a higher percentage of the FRPs' tensile strength to be mobilized. Moreover, in an NSM application the FRP reinforcement is protected (both mechanically and thermally) by the surrounding concrete, thus providing protection against freeze/thaw cycles, elevated temperatures, fire, ultraviolet radiation, and vandalism. NSM strengthening systems are also typically characterized by improved ductility [6]. Indeed, authors observed brittle debonding failures of EBR FRP strips that occurred at load levels significantly below that measured for beams strengthened with NSM CFRP reinforcing bars or strips. Similarly, Foret & Limam [7] tested both EBR and NSM CFRP strengthened two-way acting reinforced concrete slabs and observed enhanced pseudo-ductility comparing NSM to EBR. Debonding failure occurred in both

cases, although it was more sudden for EBR than for NSM. Since a higher amount of carbon was used in the EBR system for about the same average bearing capacity, the authors concluded that the NSM system was more economical than the EBR.

The efficiency of NSM FRP strengthening depends on various parameters, including the concrete and FRP materials' respective mechanical properties, the dimensions and surface treatments of the grooves, the geometry of the FRP bars, the position of the FRP within the groove, and the type of bonding agent. Several studies have presented bond tests on NSM systems and have shown that the bond between concrete and FRP is highly efficient in case where epoxy adhesives are used [1]-[17]. Few studies have been presented in the literature using cementitious bonding agents [11] [18] [19] [21], probably because typical cementitious bonding agents are (justifiably) considered to be less effective at ambient temperatures than typical epoxy systems. However, cementitious grout adhesives can be used effectively [20].

One key reason researchers have sought to use cementitious bonding agents rather than epoxies is that NSM FRP systems with cementitious adhesives may perform better at elevated temperatures [22][23][24]. This is because: (a) cementitious grout are presumed to be less affected by elevated temperatures than typical epoxies; (b) cementitious grout can provide additional thermal protection to the FRP; and (c) the polymer matrix of typical FRP bars and strips, which are normally manufactured by pultrusion, have glass transition temperatures (T_g) higher than the in-situ cured epoxy resins that are used in conventional NSM FRP strengthening applications.

This paper presents an experimental program that investigates the bond-slip behaviour of NSM FRP strengthening systems for both epoxy and cementitious bonding agents. Pull-out tests are presented on concrete specimens with an embedded carbon FRP NSM strengthening system; the specific FRP system studied was developed specifically to address the poor performance of conventional FRP strengthening systems at elevated temperatures. The influence on bond behaviour of the type of bonding agent, bond length, and bar position in the groove is investigated. Also the benefit of a ribbed surface on the FRP bars is shown.

2 EXPERIMENTAL PROGRAM

The experimental program consisted of 22 tests on prismatic concrete blocks of width, b_c = 160 mm and depth, d_c = 200 mm with embedded NSM strengthening. The blocks were cast from a single batch of concrete (Table 1 shows the mix design). Tests on cylinders 200 mm high and 100 mm in diameter were at 28 days and at 63 days (bond tests days), gave the results given in Table 2. The blocks were bonded with a specific carbon FRP NSM system (called *FireStrong*[1]) which consists of a pultruded round carbon FRP bar with a nominal diameter of 8 mm (see Figure 1) and a manufacturer specified ultimate tensile strength of 1750 MPa and elastic modulus of 136 GPa. The total length of each bar was, L_c = L_b+2 L_{free}+300 mm, where L_{free} is the unbonded length of the bar, semi-arbitrarily set to 50 mm, and L_b is the bonded length of the bar within the NSM groove (see Figure 2).

Table 3 shows the experimental program, whereby two repeated bond tests for each parameter investigated were carried out. Tests were undertaken by varying the following parameters:

- the bonding length (Figure 2), L_b (300 mm; 400 mm);
- the dimensions of the NSM groove, $b_g x b_g$ (16x16 mm^2, Figure 3a,b; 20x20 mm^2, Figure 3c);
- the position of the bar inside the groove (top surface - Figure 3a,c; centre - Figure 3 2b);
- the bonding agent (*FireStrong Grout*[2] cementitious; *Adesilex PG1*[2] epoxy adhesive); and
- the surface treatment (ribbed; smooth).

Figure 3 also shows the position of the steel bars with dashed circle lines. The eccentricity between the FRP bars embedded in the adhesive and the steel bar is reasonably small. As such, this is considered to not significantly affect the strain distribution in the FRP bars. No rotation of the specimen were observed during similar tests in the past [17].

[1] Specific product names are given simply for the purposes of factual accuracy, and should not (necessarily) be construed as an endorsement of the systems quoted.
[2] Specific product names are given simply for the purposes of factual accuracy, and should not (necessarily) be construed as an endorsement of the systems quoted.

Table 3 gives the groove perimeter, p_g, and the shape ratio, *k*, defined as $\frac{b_g}{d}$ [25]. Note that the two specific groove dimensions in the current study were chosen so that the shape ratio, *k*, would be greater than 1.5 so as to avoid splitting failures in the concrete cover [25].

2.1 Fabrication

The concrete blocks were cast in steel formwork as shown in Figure 4. After curing, a 'wall chaser' (called a 'tuckpointing grinder' in North America) with two parallel diamond cutting discs was used to cut vertical slots in the bottom concrete cover of the blocks. The remaining fin of the concrete cover material was removed with a break-out tool. The groove was then made smooth and clean, and the bar was placed within the groove and grouted using either cementitious grout (see Figure 5a) or epoxy resin (see Figure 5b). Figure 6 shows the specimens after the preparation.

Note that the strengthening system was easily realized placing the beam upside down. However, even if the cementitious matrix is not thixotropic, the strengthening technique is quite easy to realize also in real buildings, according to the installation guide provided by Milliken (Zeiler, 2013 [26]). The cementitious grout is a pumpable grout, high flow, unsanded, especially formulated for the grouting of bars in the typical groove of the NSM strengthening system. Compression tests of the cementitious grout were carried out. The grout was mixed in a high-speed mixer with the prescribed volume of potable water, until a uniform consistency was achieved, according to the Contractor Training Manual. The water/cement ratio of the mix was set equal to 0.23, according to the manufacturer technical data sheet. The tested specimen was a cylinder, 100 mm high and 50 mm diameter. The compression test was carried out through the 810 Material Testing Machine (MTS). The failure load of the tested specimen was 176 kN, therefore the ultimate strength of the grout is about 90 MPa, which is in accordance with the compressive strength at 28 days, provided by the manufacturer.

When using epoxy bonding agent, the grooves' surfaces were also treated with a primer (*Mapewrap*[2] primer), as recommended by the epoxy manufacturer. Smooth bars were created by the authors by

manually eroding the polymeric rib surface ribs from the commercially available carbon FRP bars that were used.

2.2 Instrumentation

Local measurement of strains along the bonded length of the FRP bars was accomplished by bonding foil strain gauges (length = 12mm) at five locations on the carbon FRP bars before they were placed and bonded inside the grooves. The spacing between the strain gauges was either 70 mm or 90 mm for the cases with L_b equal to 300 mm (Figure 7 a) or 400 mm (Figure 7 b), respectively. The presence of the strain gauges is not expected to significantly influence the bond response or performance [27]. Finally, cylindrical steel anchors were installed on the ends of the FRP bars (Figure 8), and filled with *MAPEI Epojet*[3] epoxy resin to ensure adequate anchorage of the free end of the FRP bars in the testing machine.

2.3 Test setup

Various researchers have used different test setups to characterize the bond behaviour of NSM strengthening systems for concrete, and a standard procedure has yet to be defined and agreed; however it is well known that the testing procedure may influence the observed bond performance and failure loads observed [[28], [29], [30]].

The test setup used in the current study (see Figure 9) was a single lap shear test (SST) that has previously been adopted by the authors for other pull-out tests on NSM and EBR strengthening systems [12]; it is considered by the authors to be reliable and is also commonly used by others [8, 18-23]. Indeed, a recent round-robin bond pull-out testing initiative concluded that the SST setup used is preferable to other testing methods as a standard test method for characterizing the bond response and capacity of NSM FRP strengthening systems [11].

[3] Specific product names are given simply for the purposes of factual accuracy, and should not (necessarily) be construed as an endorsement of the systems quoted.

The SST setup was used to load the FRP bars in tension with the concrete prism attached at the base of a universal materials testing frame using two steel bars with 20 mm diameter (Figure 9). These bars were embedded within the concrete prism (Figure 4), and bolted to a steel plate that was rigidly linked to a lower steel plate and clamped into the lower grips of the testing frame (Figure 9). Figure 9 indicates that two opposite sides of each concrete prism were bonded with an NSM bar, so as to increase the possible number of tests whilst minimizing the total number of specimens,, however each NSM strengthened face was tested separately. All tests were performed in a crosshead displacement control mode at a rate of 0.015 mm/s. Tests were performed at temperature ranging between 20°C and 35°C. Therefore, we have no temperature effect on the bond.

3 TESTS RESULTS

3.1 Failure mode and loads

Figure 10a to 10d show representative test specimens after pull-out testing, highlighting that the failure occurred due to debonding at the FRP Bar/Adhesive (B/A) interface under the maximum load, P_{max}, except for one specimen for which explosive failure of the concrete block (C) occurred. Table 4 summarizes the P_{max} values obtained for all specimens, and also summarizes the peak values of the local shear stress, τ_{max}, which gives an indication of the quality of the bond.

Peak values of the local bond shear stress, τ_{max}, were evaluated based on strains recorded by strain gauges 1 and 2 (see Figure 7), since between those gauges the strains were typically at their maximum values. Generally, the shear stress between two strain gauges (*i* and *i*+1 in Figure 11) can be calculated based on the simple force equilibrium equation:

$$\tau_{i,i+1} = \frac{E_f A_f}{p_f} \frac{(\varepsilon_{i+1} - \varepsilon_i)}{(z_{i+1} - z_i)} \quad (1)$$

where z_i and z_{i+1} define the location of the strain gauges *i* and *i*+1, with i ranging between 1 and 4; ε_i and ε_{i+1} are the local measurements of the strain respectively in z_i and z_{i+1}; $E_f A_f$ is the axial stiffness of the FRP; p_f is the perimeter of the bonded bar, since the failure occurred due to the debonding at

bar/adhesive interface. Due to the low distance between the strain gauges, the error is not so big even if more refine method could be used to define the "shear stress – slip law" [31]. The ratio between the values of P_{max} recorded for two equal specimens is not always proportional to the ratio between the corresponding τ_{max} values (see Table 4), which are a local measure.

The measurement of the strains also enables the calculation of the slip, $s_{i,i+1}$, corresponding to the shear stress, $\tau_{i,i+1}$. The slip was calculated by integrating the strain from the unloaded end of the bond, i.e. Strain Gauge 6, to the loaded end, i.e. Strain Gauge 0 (see Figure 7), where the theoretical strain, ε_0, assumes the following peak value:

$$\varepsilon_0 = \frac{P}{E_f A_f} \tag{2}$$

Thus, the slip $s_{i,i+1}$ can be evaluated as:

$$s_{i,i+1} = \sum_{k=i}^{n} (z_{k+1} - z_k)\left(\frac{\varepsilon_k + \varepsilon_{k+1}}{2}\right) \tag{3}$$

where *n* is the total number of strain gauges, which is 5 in this case.

More details on the calculation of the "shear stress – slip law" can be found in [31].

3.2 Bonding agent

The applied load (P) versus crosshead displacement (Δ) of the testing frame was recorded during all tests. For specimens L_b*300-*b_g*16-T-R-R* and L_b*300-*b_g*20-T-R-R,* respectively, Figure 12a and 12b show that P_{max} was about 50 kN. After attaining P_{max}, the $P - \Delta$ curves show subsequent lower peaks, ranging between 20 kN and 40 kN (i.e. 40-80% of $P_{u,\mathrm{exp}}$); these represent a sort of residual strength, or additional energy dissipation, likely based on the interlocking mechanism between the adhesive resin and the ribbed bar surface.

Conversely, for specimens L_b*300-*b_g*16-T-CM-R* and L_b*300-*b_g*20-T-CM-R*, Figure 12a and 12b show that P_{max} was considerably lower for bars bonded with cementitious bonding agent compared to that obtained for resin bonded bars, and equal to about 25 kN. In these cases, the

specimens failed to retain any significant strength beyond the peak load; only about 24% of $P_{u,\exp}$. To evaluate the post-peak bond response the specimens were tested until the very high slip values, of more than 30 mm, were achieved. Secondary failure was also observed at large bond slip displacements in the adhesive/concrete interface after the main debonding at B/A interface.

It is noteworthy that the efficiency of the cementitious-bonded NSM strengthening system, defined as ratio between the debonding load and the theoretical ultimate tensile load of the FRP bars themselves, is about 28%. Thus, this strengthening is more efficient than common EBR CFRP plates, which efficiency ranges typically between 11 and 19% [12].

3.3 Surface treatment

Figure 12 shows the load plotted against the slip, allowing a comparison between strengthening systems with ribbed versus smooth bars. The maximum load attained with ribbed bar cementitious bonded strengthening system is 2 to 2.5 times that attained using smooth bars, whereas there is no noticeable difference between smooth and ribbed bars for the resin bonded strengthening system.

3.4 Position

Figure 12c shows that the position of the bar (top or centre) of the grove appears to not have any clear influence on the bond behaviour of the strengthening system when smooth bars are used. When ribbed bars are used and placed at the top of the groove, the bond behaviour is better than that observed by placing the bar in the centre of the groove (red curves are always under the black curves in Figure 12a). This is due to the low amount of matrix, between two consecutive ribs of the bar and the top surface of the groove, involved in the strut and tie mechanism, which leads to a stronger mechanism when the bar is at the top (Figure 13a) rather than in the centre (Figure 13b). The bond behaviour observed in all the tests was mainly cohesive up to attainment of the maximum load, the value of which was not obviously affected by the position of the bar within the groove.

3.5 Dimension of the groove

Figure 12 shows that the dimension of the groove does not significantly affect the bond response for the systems tested herein. Preliminarily, this appears to be in contrast to that shown by Bilotta et al. [32], who performed an NSM bond testing program using an identical testing setup, specimens with the same shape and dimension, the same bonding length, a smooth CFRP bar with approximately the same elastic modulus, a different commercial resin as bonding agent, and a very poor concrete representative of the properties of existing structures. They found that the efficiency of the NSM was controlled by the groove dimension, which affected the maximum load achieved. Moreover, the poor properties of the concrete they used affected the failure mode, which occurred at the adhesive/concrete interface, whereas in the experimental program presented in this paper the failure generally occurred by debonding at the B/A interface, because a high strength concrete was used. Thus, it is likely that the maximum load does not increase with the dimension of the groove when failure is by debonding at the B/A interface.

Figure 12 cannot give any information about the stiffness of the strengthening system, since the crosshead displacement is not fully representative of the bond at B/A interface due to the slip between the anchorage and the grip, as well as the elastic elongation of the FRP unbonded length. However, the P versus s curve allows the stiffness of the strengthening system to be defined. Note that s was calculated by integrating the strain from the unloaded end to the loaded end, in Figure 7 and according to Eq. (3).

Figure 14a and 14b depict P versus s curves for specimens L_b300-b_g16-T-R-R and L_b300-b_g20-T-R-R, showing that the dimension of the groove does not affect the bond stiffness of the strengthening system, or the maximum load. A similar result was obtained from specimens L_b300-b_g16-T-CM-R and L_b300-b_g20-T-CM-R. This confirms previous results for epoxy bonded strengthening systems [32]. Figure 14a, 13b, and 13c, show comparisons between L_b300-T-CM-R and L_b300-T-R-R, showing that strengthening with resin is stiffer than that with cementitious mortar.

To assess the effective bond length of the analysed strengthening systems, the strain measured by the strain gauges, placed as shown in Figure 7a, were plotted versus the abscissas z, for different values of the applied load. The slope of these curves represents the capacity of the strengthening system to transfer the shear stress from the loaded end for the FRP (where the theoretical strain, ε_0, is assumed), to the unloaded end; the higher the slope of this line, the higher the capacity to transfer stress. Since the failure mode was by debonding at B/A interface, over about the 70-80% of P_{max}, the strain gauges had stopped working at these levels, thus the profile of strains along the bonded length could not be calculated in this load range. Comparing the strain profiles $\varepsilon(z, P)$ obtained referring to L_b*300-T-CM-R* (Figure 15 a-b) versus those obtained referring to L_b*300-T-R_R* (Figure 15c-d), it is clear that when the cementitious adhesive is used a greater bonded length is needed to obtain the maximum possible bond capacity. For example, comparing $\varepsilon(z, P = 18\ kN)$ for L_b*300-*b_g*16-T-CM-R-02* (Figure 16a) with that for L_b*300-*b_g*16-T-R-R-01* (Figure 15c), it can be seen that when the cementitious adhesive is used a bonded length of 300 mm is needed, whereas 150 mm of bond length is sufficient when epoxy resin adhesive is used.

Finally, the shear stress $\tau_{1,2}$, which was calculated according to Eq. (*1*), was plotted versus the corresponding slip $s_{1,2}$. Figure 16a shows that the shear stress for L_b*300-*b_g*16-T-R-R* is zero when the slip is about 0.8 mm, whereas the shear stress for L_b*300-*b_g*20-T-R-R* (Figure 16b), after the peak value, slightly decreased however did not attain a zero value. The τ versus s behaviour for L_b*300-T-CM-R* (Figure 16d) was significantly different from L_b*300-T-R-R*. By comparing the strengthening systems L_b*300* and L_b*400*, it is noteworthy that an increase in the bonding length of about 33% leads to an increase in the maximum load of about 12%.

Figure 16 also shows that in case of an epoxy resin bonded strengthening system, the shear stress usually attains a peak value, the coordinates of which are τ_{max}-s_{max}, followed by a softening branch. If the FRP bar is placed in the centre of the groove, the peak value of the shear stress is slightly higher than that obtained when the bar is placed on the top of the groove, however the slope

of the softening branch is also high. By comparing the strengthening systems with smooth and ribbed bars, it is noted that the stiffness of the strengthening system with smooth bars is lower, and the amount of slip is greater than that recorded for the strengthening system with ribbed bars.

The interpretation of the τ versus s behavior of the cementitious bonded strengthening system (Figure 16) is not clear due to scatter in the results. However, it is noteworthy that it does not seem to be a softening branch, and the pseudo-constant curve in the post-elastic stage (after the peak) may indicate a frictional bond behavior.

CONCLUSIONS

Available research on the behaviour of cementitious-bonded near surface mounted FRP strengthening systems for concrete is currently limited, most likely because cementitious bonding agents for NSM FRP applications are rightly considered less effective at room temperature than competitor epoxy adhesive systems. The experimental results from the current study have shown that whilst this is true:

- the bond of the cementitious-bonded system has less strength and stiffness as compared with the epoxy resin-bonded NSM system, however the performance of the cementitious-bonded NSM CFRP ribbed bar is comparable with common EBR CFRP plates in terms of the utilisation of the FRP material;
- the cementitious bonded NSM FRP strengthening system is effective if ribbed bars are used, otherwise the efficiency of the system is comparatively low;
- the dimension of the grooves (2 to 2.5 times the bar's diameter) does not appear to have any obvious influence on the bond stiffness and debonding load for the systems tested, since the main failure mode of the strengthening system was the debonding at bar/adhesive interface;
- a greater bonding length (33% greater) provides an increase of the maximum load of about 12% for the cementitious bonded NSM FRP system; and
- the position of the bar in the groove has a minor influence when ribbed FRP bars are used with the cementitious bonded system; when the bar was placed in the centre of the groove the debonding load was 27% lower than that obtained by testing the strengthening system with the bar positioned at the top of the groove.

Experimental data will be used to calibrate FE models in future research.

REFERENCES

[1] Rami A. Hawileh, Hayder A.Rasheed, Jamal A.Abdalla, Adil K.Al-Tamimi (2013) Behavior of reinforced concrete beams strengthened with externally bonded hybrid fiber reinforced polymer systems. Materials & Design Volume 53, January 2014, Pages 972-982

[2] Elias I. Saqan, Hayder A. Rasheed, Rami A. Hawileh (2013) An efficient design procedure for flexural strengthening of RC beams based on ACI 440.2R-08. Composites Part B: Engineering Volume 49, June 2013, Pages 71-79

[3] R.A. Hawileh, W. Nawaz, J.A. Abdalla (2018) Flexural behavior of reinforced concrete beams externally strengthened with Hardwire Steel-Fiber sheets Construction and Building Materials Volume 172, 30 May 2018, Pages 562-573

[4] Ahmed Al-Abdwais, Riadh Al-Mahaidi. (2016). Bond behavior between NSM CFRP laminate and concrete using modified cement-based adhesive."Construction and Building Materials, 127:pp. 284-292

[5] Ahmed Al-Abdwais, Riadh Al-Mahaidi. (2017). Bond properties between carbon fibre reinforced polymer (CFRP) textile and Concrete using modified cement-based adhesive, "Construction and Building Materials, 154: p.p. 983-992.

[6] El-Hacha R., Rizkalla S: H., (2004). Near-Surface-Mounted Fiber-Reinforced Polymer Reinforcements for Flexural Strengthening of Concrete Structures. ACI Structural Journal, September-October 2004, 717-726

[7] Foret G., Limam O., (2008). Experimental and Numerical analysis of RC two-way slabs strengthened with NSM CFRP rods. Construction and Building Materials 22 (2008) 2025-20

[8] De Lorenzis L., Nanni A., La Tegola A., (2000). Strengthening of Reinforced Concrete Structures with Near Surface Mounted FRP Rods., PLAST 2000, Milan, Italy, May 9-11, 1-9.

[9] Teng J.G., de Lorenzis L., Wang B., Li R., Wong T.N., Lam L., (2006). Debonding failures of RC beams strengthened with near surface mounted CFRP Strips. Journal of composites for construction 10, no. 2, 92–105.

[10] Castro E. K., Melo G. S., Nagato Y., (2007). Flexural strengthening of RC “T” beams with NSM FRP reinforcements. FRPRCS-8, University of Patras, Patras, Greece, July 16-18, 2007

[11] Burke P.J., (2008). Low and High Temperature Performance of Near Surface Mounted FRP Strengthened Concrete Slabs. Master thesis, Queen’s University, Kingston, Ontario, Canada

[12] Bilotta A., Ceroni F., Di Ludovico M., Nigro E., Pecce M., (2011). Bond Efficiency of EBR and NSM FRP Systems for Strengthening Concrete Members. J. Compos. Constr. 2011.15:757-772

[13] Costa I., Barros J., (2011). Assessment of the bond behaviour of NSM FRP materials by pullout tests. First Middle East Conference on Smart Monitoring, Assessment and Rehabilitation of Civil Structures, Dubai

[14] Ceroni F., Pecce M., Bilotta A:, Nigro A (2012). Bond behavior of FRP NSM systems in concrete elements. Composites: Part B 43, 99–109

[15] Wu G.; Dong Z. Q., Wu Z. S., Zhang L. W., (2013). Performance and Parametric Analysis of Flexural Strengthening for RC Beams with NSM-CFRP Bars. J. Compos. Constr. DOI: 10.1061/(ASCE)CC.1943-5614.0000451. © 2013 American Society of Civil Engineers

[16] Bilotta A., Ceroni F., Nigro E., Pecce M.,. (2015) Efficiency of CFRP NSM strips and EBR plates for flexural strengthening of RC beams and loading pattern influence. Composite Structures, Volume 124, Pages 163–175, doi:10.1016/j.compstruct.2014.12.046

[17] Bilotta A., Ceroni F., Barros J.A.O., Costa I., Palmieri A., Szabo K.Z., Nigro E., Matthys S., Balazs G.L., Pecce M., (2015). "Bond of NSM FRP strengthened concrete: round robin test initiative", Journal of Composite for Construction (ASCE)

[18] El-Gamal S., Al-Salloum Y., Alsayed S., Aqel M., (2012). Performance of near surface mounted glass fiber reinforced polymer bars in concrete. Journal of Reinforced Plastics and Composites, 31 (22) 1501–1515 DOI: 10.1177/073168441246408

[19] Palmieri A., Matthys S., Taerwe L., (2012). Double Bond Shear tests on NSM FRP strengthened members. Proceedings of CICE 2012, Rome, Italy, June 13-15, 2012

[20] G. Loreto, L. Leardini, D. Arboleda, A. Nanni, (2014). Performance of RC Slab-Type Elements Strengthened with Fabric-Reinforced Cementitious-Matrix Composites. Journal of Composites for Construction. Volume 18 Issue 3.

[21] Burke P.J., Bisby L. A., Green M., (2013). Effects of elevated temperature on near surface mounted and externally bonded FRP strengthening systems for concrete. Cement & Concrete Composites 35, 190–199

[22] Di Tommaso, A.; Neubauer, U.; Pantuso, A.; and Rostásy, F.S., (2001), Behavior of adhesively bonded concrete-CFRP joints at low and high temperatures. Mechanics of Composite Materials, V. 37, No. 4, pp. 327-338.

[23] Michels J., Widmann R., Czaderski CH., Allahvirdizadeh R., Motavalli M. (2015). Glass transition evaluation of commercially available epoxy resins used for civil engineering applications, Composites Part B, 77, 484-493

[24] Michels J., Sena Cruz J., Christen R., Czaderski Ch., Motavalli M. (2016). Mechanical performance of cold-curing epoxy adhesives after different mixing and curing procedures, Composites Part B 98, 434-443.

[25] De Lorenzis L., Teng JG., (2007). Near-surface mounted FRP reinforcement: an emerging technique for structural strengthening. Compos Part B: Eng 2007;38:119–43

[26] Zeiler B. (2013). FireStrong: Installation Guide & Contractor Training Manual

[27] Seracino R, Jones NM, Page MW, Ali MSS, Oehlers DJ, (2007). "Bond strength of near surface mounted FRP-to-concrete joints", ASCE J Compos Constr;11(4):401–9

[28] Aiello M.A., Leone M., (2008). “Interface analysis between FRP EBR system and concrete”, Composites: Part B 39 (2008) 618–626

[29] Novidis, D. G., and Pantazopoulou, S. J. (2008). Beam pull out tests of NSM—FRP and steel bars in concrete, Proc., CICE 2008, Zurich, Switzerland

[30] Yao, J., Teng, J. G., and Chen, J. F. (2005). “Experimental study on FRP-to-concrete bonded joints.” Compos., Part B, 36(2), 99–113

[31] A. Bilotta, C. Faella, E. Martinelli, and E. Nigro. (2012) Indirect Identification Method of Bilinear Interface Laws for FRP Bonded on a Concrete Substrate. Journal of Composites for Construction, Vol. 16, No. 2, April 1, 2012. ASCE, ISSN 1090-0268/2012/2-171–184. DOI: 10.1061/(ASCE)CC.1943-5614.0000253

[32] Bilotta A., Ceroni F., Nigro E., Pecce M., (2014). Strain assessment for the design of NSM FRP systems for the strengthening of RC members, Construction and Building Materials 69 (2014) 143–158

[33] Del Prete I., Bilotta A., Bisby L., Nigro E., (2015). Flexural tests on RC beams strengthened with NSM FRP bars bonded with cementitious grout. The 12th International Symposium on Fiber Reinforced Polymers for Reinforced Concrete Structures (FRPRCS-12) & The 5th Asia-Pacific Conference on Fiber Reinforced Polymers in Structures (APFIS-2015) Joint Conference, 14-16 December 2015, Nanjing, China

[34] Chen JF, Yang ZJ, Holt GD, (2001). “FRP or steel plate-to-concrete bonded joints: effect of test methods on experimental bond strength”. Steel Compos Struct 2001; 1(2):231–44

[35] Wu Z. S., Yuan H., Yoshizawa H., and Kanakubo T., (2001). “Experimental/analytical study on interfacial fracture energy and fracture propagation along FRP-concrete interface.” SP-201-8, American Concrete Institute, Farmington Hills, MI, 133–52

[36] Savoia M., et al. (2009). “Experimental round robin test on FRP concrete bonding.” Proc., 9th FRPRCS, American Concrete Institute, Farmington Hills, MI

[37] Ferracuti B., Mazzotti C., and Savoia M. (2008). “A new single-shear set-up for stable delamination tests on FRP-concrete joints”, Constr. Build. Mater., 23(4), 1529–1537

[38] Dai J., Ueda T., Sato Y. (2005). “Development of the nonlinear bond stress-slip model of fiber reinforced plastics sheet—Concrete interfaces with a simple method.” J. Compos. Constr., 9(1), 52–62

Table 1. Concrete batch

Component	**Quantity (per $1m^3$)**
Cement (CEM_II_42.5_R)	380 kg
Sand	1456 kg
Aggregate 4/10 mm	825 kg
Superfluid (Chryso Premia 180)	4800 ml
Water	175 l
Water/Cement	0.46

Table 2. Concrete compression tests results

Age	Label	f_c (MPa)	f_{cm} (MPa)
28 days	C1	44.91	46.24
	C2	47.33	
	C3	46.48	
63 days (Bond test days)	C1	49.06	48.29
	C2	48.54	
	C3	47.27	

Table 3. Test Matrix

Label	n	L_b (mm)	L_c (mm)	b_g (mm)	Bar surface	Bonding agent	Bar position	p_g (mm)	k
L_b300-b_g16-T-CM-R	2	300	400	16	Ribbed	Mortar	TOP	48	2
L_b300-b_g16-C-CM-R	2						CENTRE		
L_b300-b_g16-T-R-R	2					Resin	TOP		
L_b300-b_g16-C-R-R	2						CENTRE		
L_b300-b_g20-T-CM-R	2	300	400	20	Ribbed	Mortar	TOP	60	2.5
L_b300-b_g20-T-R-R	2					Resin			
L_b300-b_g16-T-CM-S	2	300	400	16	Smooth	Mortar	TOP	48	2
L_b300-b_g16-C-CM-S	2						CENTRE		
L_b300-b_g16-T-R-S	2					Resin	TOP		
L_b300-b_g16-C-R-S	2						CENTRE		
L_b400-b_g16-T-CM-R	2	400	500	16	Ribbed	Mortar	TOP	48	2

Table 4. Failure load and mode

Label	$P_{u,exp}$ (kN)	Failure mode	τ_{max} (MPa)
L_b300-b_g16-T-CM-R-01	22.85	B/A	-
L_b300-b_g16-T-CM-R-02	26.22	B/A	-
L_b300-b_g16-C-CM-R-01	20.86	B/A	2.42
L_b300-b_g16-C-CM-R-02	17.68	B/A	2.21
L_b300-b_g16-T-R-R-01	52.18	C	9.70
L_b300-b_g16-T-R-R-02	56.77	B/A	10.28
L_b300-b_g16-C-R-R-01	45.38	B/A	14.17
L_b300-b_g16-C-R-R-02	47.48	B/A	13.67
L_b300-b_g20-T-CM-R-01	25.05	B/A	1.32
L_b300-b_g20-T-CM-R-02	23.78	B/A	2.64
L_b300-b_g20-T-R-R-01	52.45	B/A	11.92
L_b300-b_g20-T-R-R-02	55.22	B/A	9.76
L_b300-b_g16-T-CM-S-01	10.32	B/A	1.24
L_b300-b_g16-T-CM-S-02	11.94	B/A	1.05
L_b300-b_g16-C-CM-S-01	9.44	B/A	1.64
L_b300-b_g16-C-CM-S-02	9.60	B/A	0.68
L_b300-b_g16-T-R-S-01	51.12	B/A	7.73
L_b300-b_g16-T-R-S-02	52.98	B/A	10.03
L_b300-b_g16-C-R-S-01	49.81	B/A	7.59
L_b300-b_g16-C-R-S-02	51.42	B/A	11.97
L_b400-b_g16-T-CM-R-01	24.47	B/A	3.54
L_b400-b_g16-T-CM-R-02	30.45	B/A	3.11

Figure 1. CFRP bar used in the current study

1

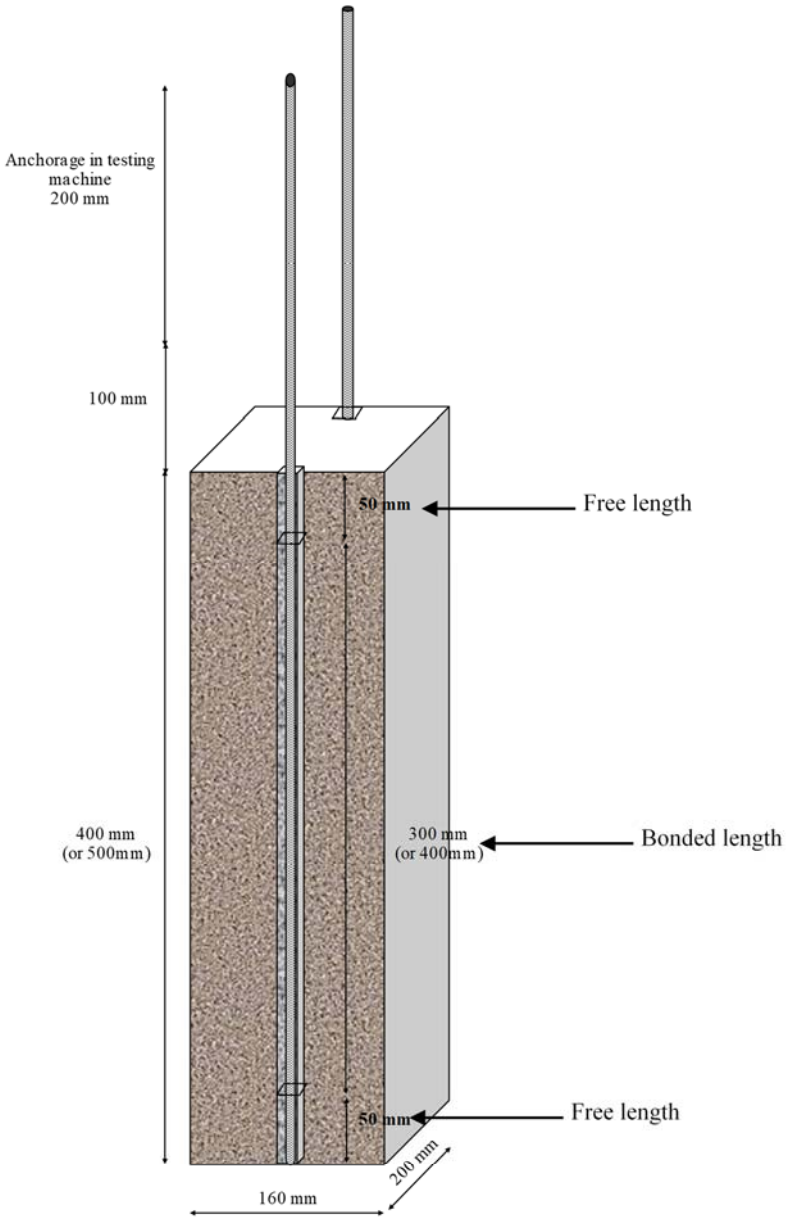

2
3 Figure 2. Isometric view
4

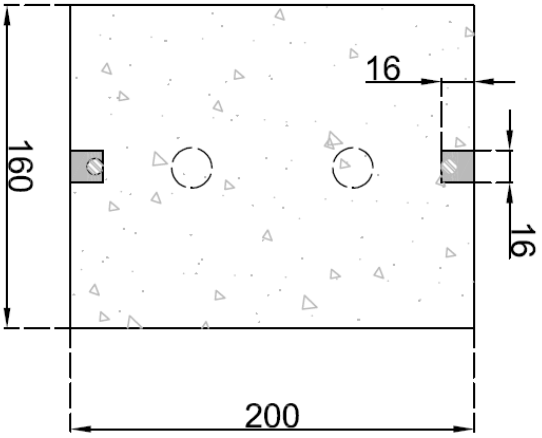

a) b_g*16-T*

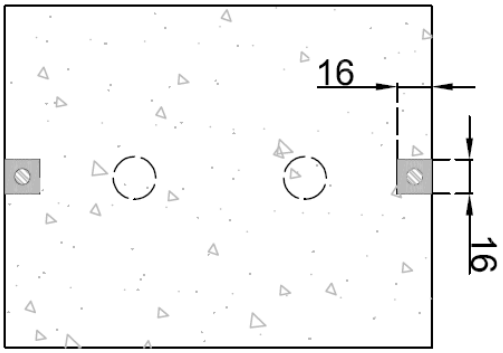

b) b_g*16-C*

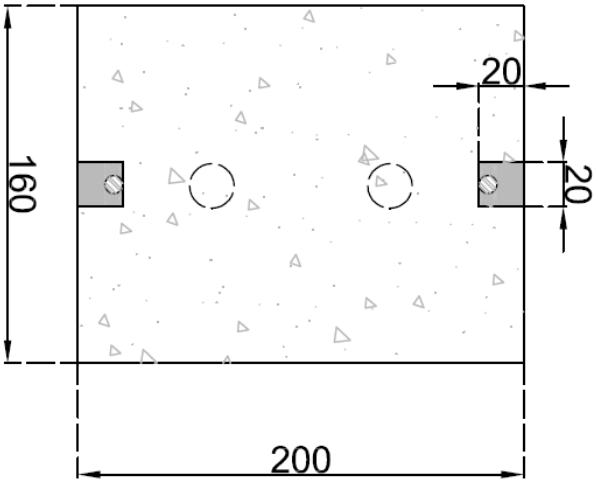

c) b_g*20-T*

Figure 3. Cross section

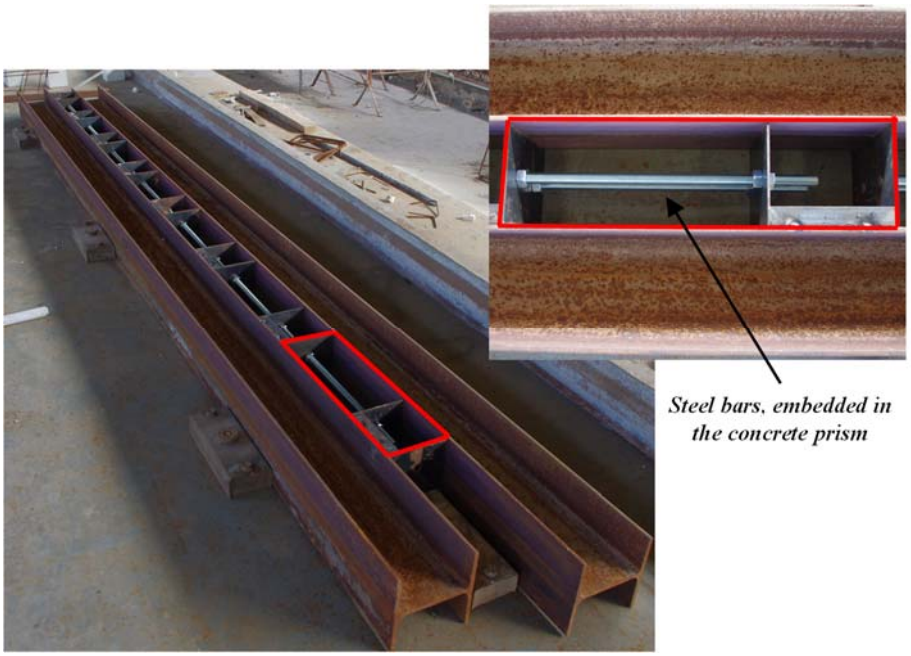

Figure 4. Concrete cast formworks

1

Figure 5a. Cast of cementitious mortar in the groove

Figure 5b. Placement of thixotropic resin in the groove

2

3

(a)  (b)  (c) 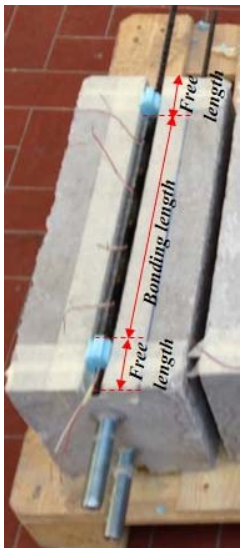

Figure 6. Specimen after the preparation: (a) cementitious grout and (b) epoxy resin) – (c) details on bond length

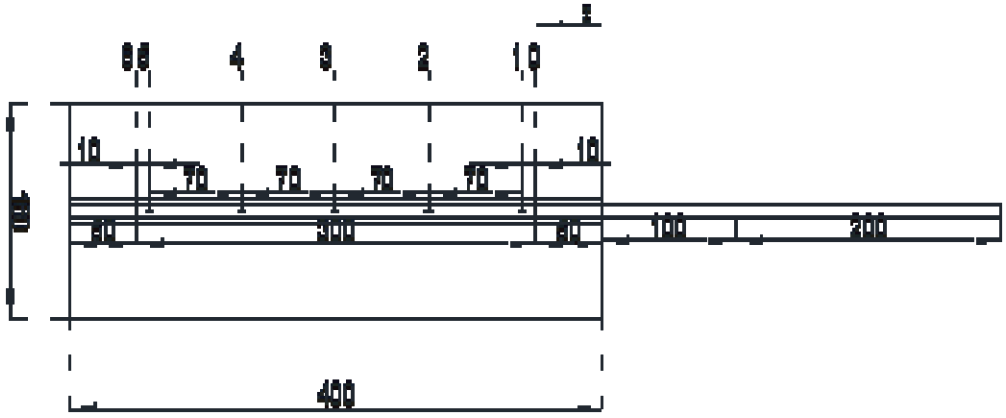

a)

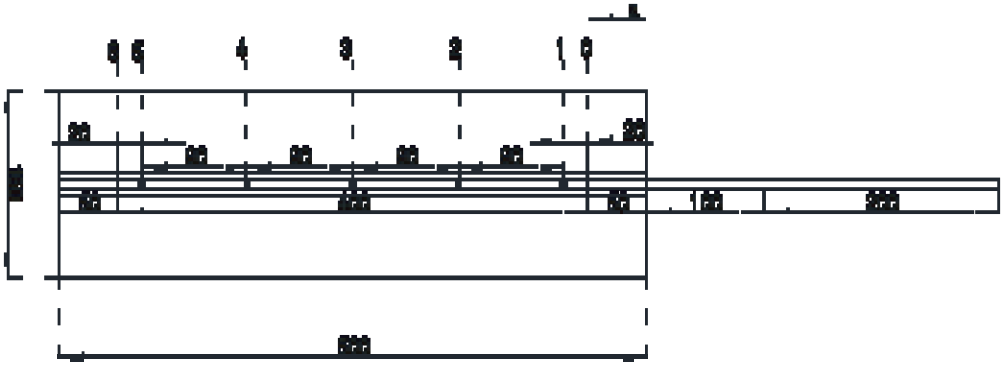

b)

Figure 7. Strain gauges locations on the carbon FRP bars: a) L_b 300 mm; L_b 400 mm

Figure 8. Installation of steel pipes on the ends of the carbon FRP bars

Figure 9. Test setup

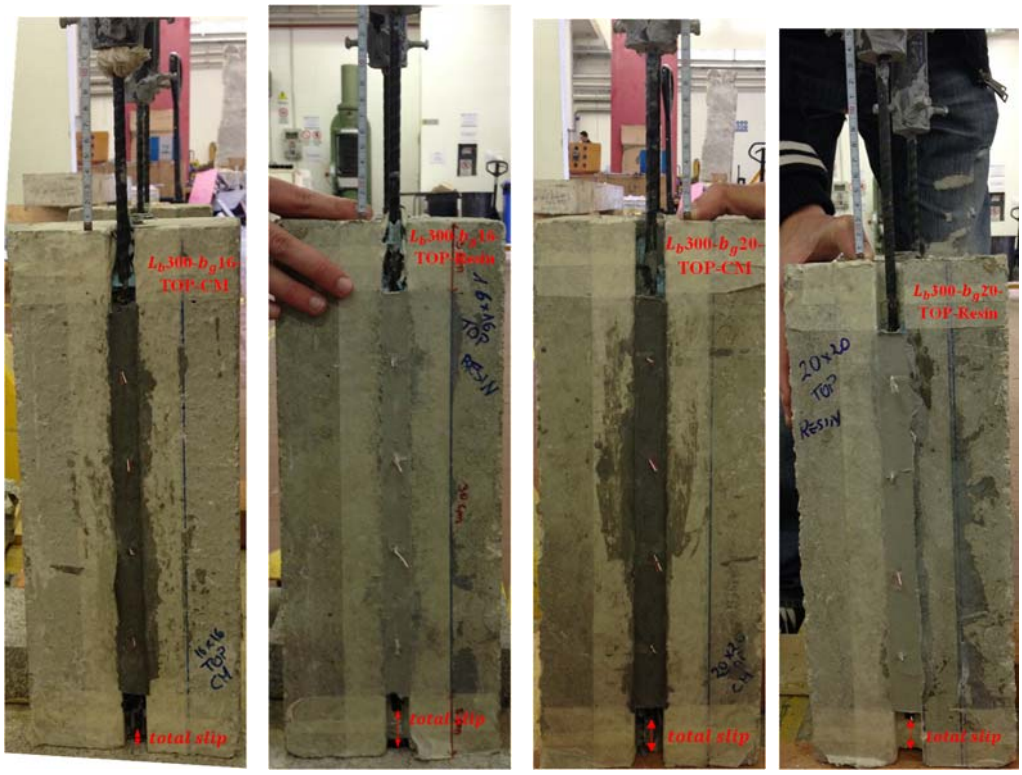

a) b) c) d)

Figure 10. Specimens after pull-out tests: a) L_b300-b_g16-T-CM; b) L_b300-b_g16-T-R; c) L_b300-b_g20-T-CM; and d) L_b300-b_g20-T-R

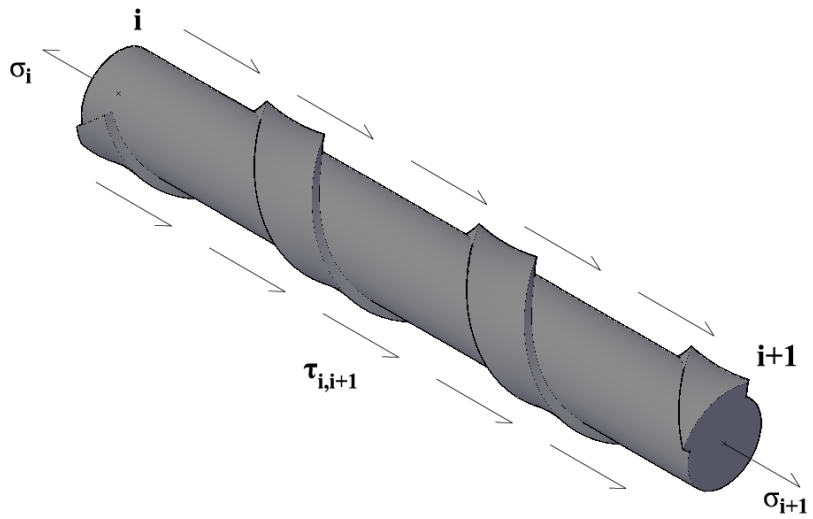

Figure 11. Schematic of local shear stresses

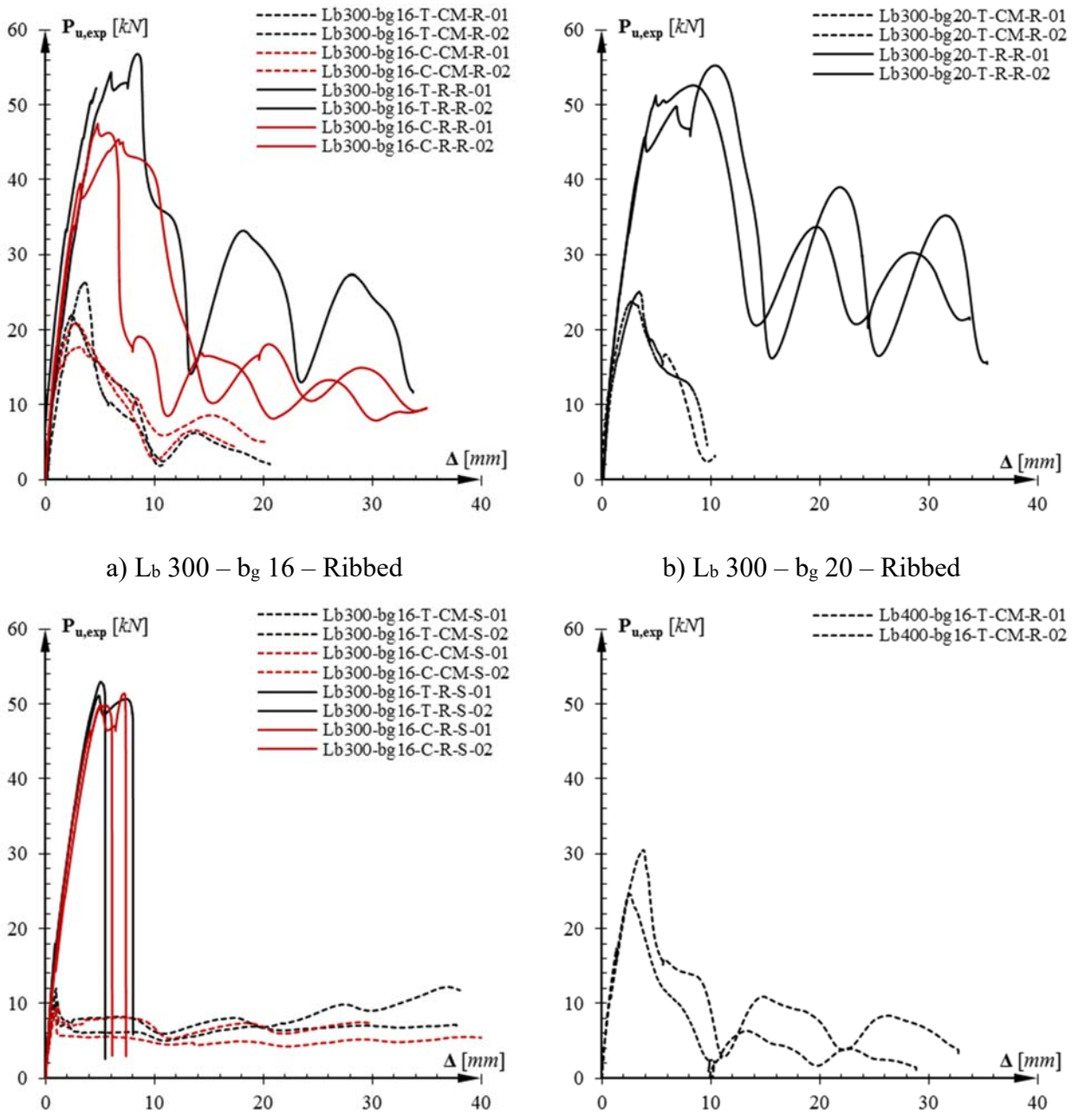

a) L_b 300 – b_g 16 – Ribbed

b) L_b 300 – b_g 20 – Ribbed

c) L_b 300 – b_g 16 – Smooth

d) L_b 400 – b_g 16 – Ribbed

Figure 12. Load versus displacement plots

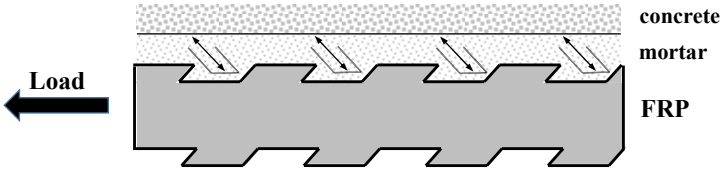

(a)

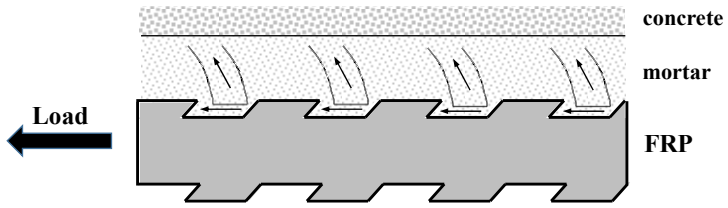

(b)

Figure 13. Strut and tie mechanism sketch (a) top bar and (b) centered bar

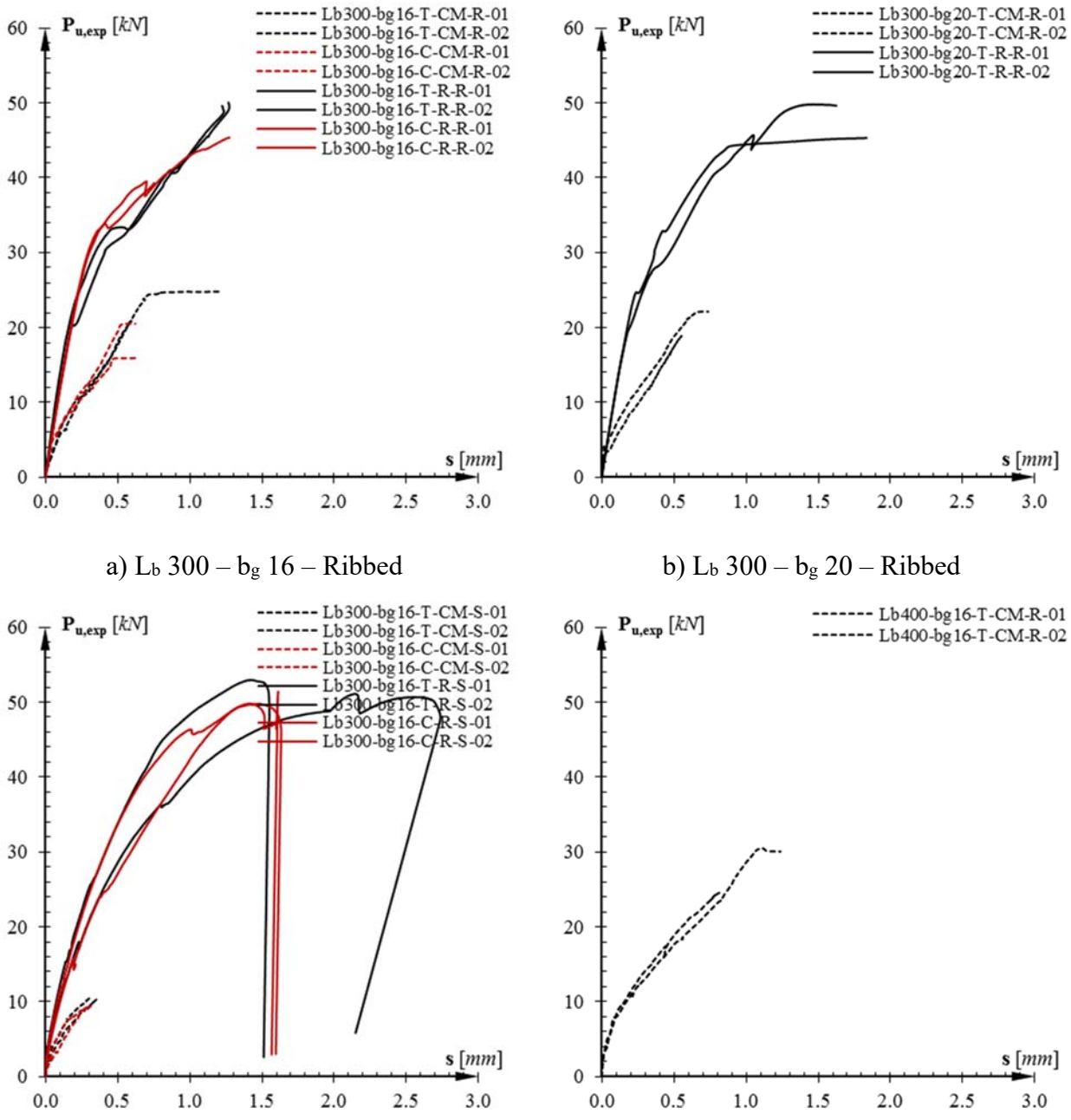

a) L_b 300 – b_g 16 – Ribbed

b) L_b 300 – b_g 20 – Ribbed

c) L_b 300 – b_g 16 – Smooth

d) L_b 400 – b_g 16 – Ribbed

Figure 14. Load versus slip plots

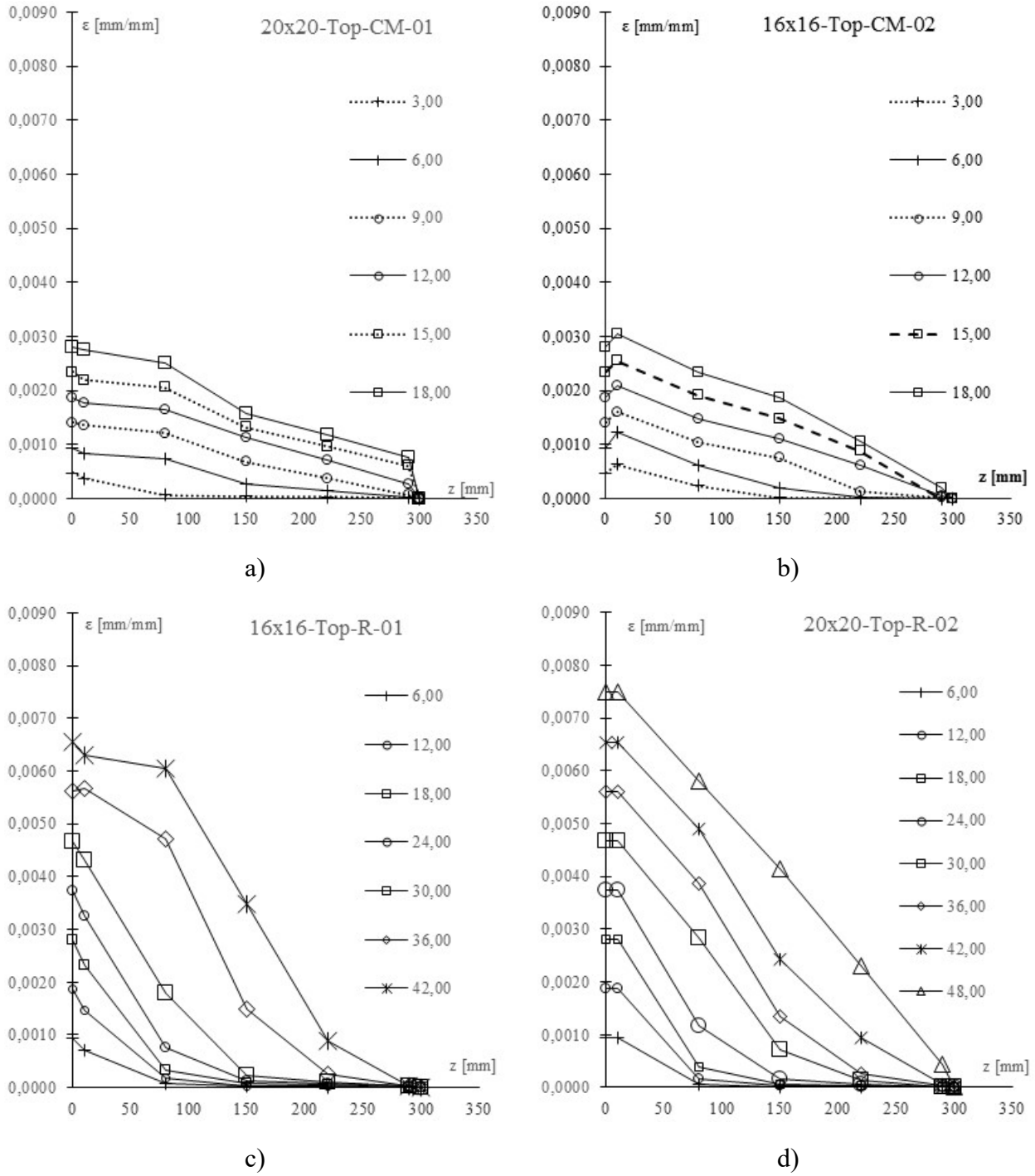

Figure 15. Strain profiles $\varepsilon(z, P)$: a) L_b300-b_g16-T-CM-R-02; b) L_b300-b_g20-T-CM-R-01; c) L_b300-b_g16-T-R-R-01; d) L_b300-b_g20-T-R-R-02

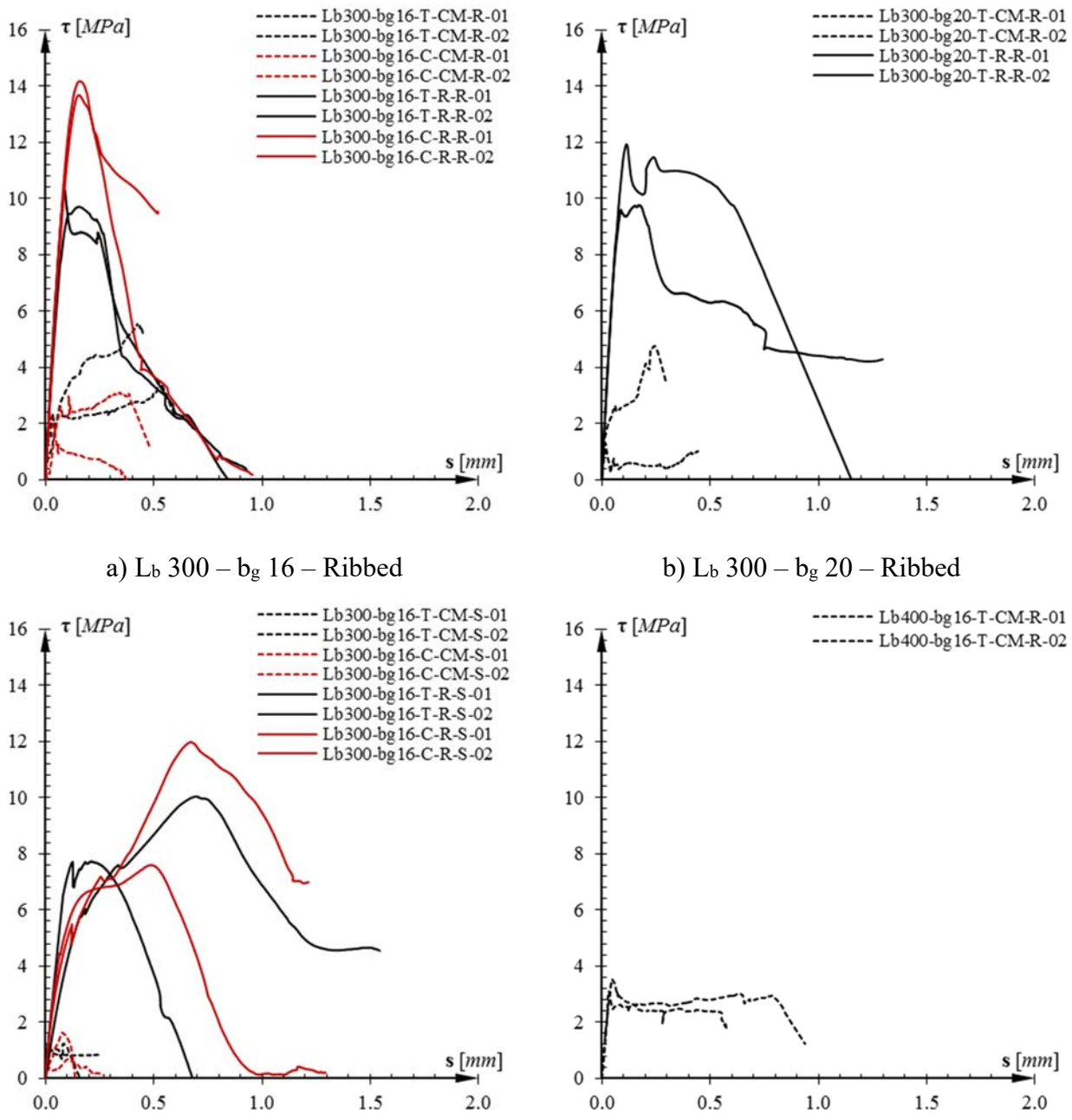

a) L_b 300 – b_g 16 – Ribbed

b) L_b 300 – b_g 20 – Ribbed

c) L_b 300 – b_g 16 – Smooth

d) L_b 400 – b_g 16 – Ribbed

Figure 16. Shear stress versus slip plots